atmosphere

Article

Advancing Heat Health Risk Assessment: Hotspot Identification of Heat Stress and Risk Across Municipalities in Algiers, Algeria

Dyna Chourouk Zitouni [1,2,3,*], Djihed Berkouk [3,4], Mohamed Elhadi Matallah [1,5], Mohamed Akram Eddine Ben Ratmia [2,3] and Shady Attia [1,*]

[1] Sustainable Building Design Lab, Department UEE, Applied Sciences, University of Liège, 4000 Liège, Belgium; elhadi.matallah@univ-biskra.dz
[2] Laboratory of Design and Modeling of Architectural and Urban Forms and Ambiances (LACOMOFA), University of Biskra, Biskra 07000, Algeria; akrameddine.benratmia@univ-biskra.dz
[3] Department of Architecture, Mohamed Khider University, Biskra 07000, Algeria; dberkouk@dah.edu.sa
[4] Department of Architecture, School of Engineering, Computing & Design, Dar Al-Hekma University, Jeddah 22246, Saudi Arabia
[5] Civil Engineering and Hydraulics Laboratory, Sustainable Development and Environment (LARGHYDE), University of Biskra, Biskra 07000, Algeria
* Correspondence: dczitouni@uliege.be (D.C.Z.); shady.attia@uliege.be (S.A.)

Abstract: With accelerating surface warming trends in urban regions, cities like Algiers are increasingly exposed to extreme heat, contributing to a growing concern over heat-related illnesses. For a comprehensive long-term assessment (2001–2023) of heat-related risks in Algiers, multi-decade satellite, meteorological, and census data were used in this study to map and assess spatial patterns of the Heat Health Risk Index (HHRI) within the framework established by the Intergovernmental Panel on Climate Change (IPCC) incorporating hazard, exposure and vulnerability components. The Universal Thermal Climate Index (UTCI) was then calculated to assess thermal stress levels during the same period. Following this, the study addressed a critical research gap by coupling the HHRI and UTCI and identified hotspots using the Getis-Ord Gi* statistical analysis tool. Our findings reveal that the intensity of HHRI has increased over time since "very-low" risk areas had an outstanding decrease (93%) and a 6 °C UTCI rise over 23 years reaching the "very strong heat stress" level. The coupled index demonstrated greater and different risk areas compared to the HHRI alone, suggesting that the coupling of both indicators enhances the sensitivity of heat risk assessment. Finally, persistently identified hotspots in central and eastern regions call for localized, targeted interventions in those areas and highlight the value of remote sensing in informing policymakers and enhancing climate resilience.

Keywords: heat vulnerability; thermal comfort; risk assessment; environmental resilience; remote sensing; climate change

check for updates

Academic Editor: Masoud Rostami

Received: 23 February 2025
Revised: 16 April 2025
Accepted: 17 April 2025
Published: 21 April 2025

Citation: Zitouni, D.C.; Berkouk, D.; Matallah, M.E.; Ben Ratmia, M.A.E.; Attia, S. Advancing Heat Health Risk Assessment: Hotspot Identification of Heat Stress and Risk Across Municipalities in Algiers, Algeria. *Atmosphere* **2025**, *16*, 484. https://doi.org/10.3390/atmos16040484

1. Introduction

Exposure to heat poses a significant threat to human health and is increasingly impacting the sustainability of urban areas, including cities in North Africa such as Algiers [1]. Ad hoc indicators have recently been introduced to track the consequences that global warming is inducing on human health [2]. The indicators are based on Crichton's [3] three key risk components: (1) hazard, which is a natural physical event that has the potential to cause discomfort or damage to vulnerable and exposed components; (2) exposure, which refers to the individual or buildings situated in locations where a potential hazard might occur; (3) vulnerability refers to how likely exposed elements are to be affected by a hazard (known as sensitivity), and also includes the ability of individuals or systems to adapt to and recover from that hazard.

By combining the three risk components via impact models, they can capture the heterogeneous set of factors and relationships linking climate change with health impacts, including heat-related mortality and changes in labor capacity [4,5]. Similarly, the Intergovernmental Panel on Climate Change (IPCC)'s Sixth Assessment Report (AR6) [4] used the three components to quantitatively analyze the spatial distribution of heat health risk (HHR). While other frameworks, such as the Climate Change and Disaster Indicators (CCDIs) developed by the Expert Team on Weather and Climate Extremes Monitoring and Assessment (ETWMO), offer alternative approaches to risk assessment, the present study adopts the IPCC's structure due to its suitability for spatial integration of environmental and socio-demographic indicators, and its compatibility with thermal stress models.

Although there have been relatively few studies following the hazard–exposure–vulnerability framework [6], the number has been increasing in recent years, with a significant concentration of research being conducted in Asia [7–11].

Geographic Information Systems (GISs) and remote-sensing technologies have an essential role in HHR assessment by providing accurate spatial and temporal data, which is crucial for mapping and analyzing the pattern of heat-related hazard, exposure, and vulnerability [10,12–15]. The literature on HHR assessment using the IPCC's framework has increasingly used remote-sensing tools to capture spatial variations in risk patterns across different regions. In 2019, the MODIS Land Surface Temperature (LST) and vegetation indices were combined with socioeconomic indicators to map HHR for the elderly in a mountainous area in China [16]. A 2020 study in the Philippines applied remotely sensed surface temperature data and social–ecological indicators to assess the current HHR [17]. Subsequently, a 2023 study in Singapore integrated remote sensing to quantify UHI intensity and coupled it with demographic data to assess the HHR for the elderly population [18]. Another 2023 study in Australia employed remote-sensing data and GIS tools to perform a comprehensive HHR assessment in Australian capital cities, incorporating health-related indicators to evaluate population sensitivity to extreme heat [19]. More recently, in 2024, a study conducted a spatially explicit assessment of the HHR in the Yangtze River Delta, China, using multi-sensor remote-sensing images [7]. Finally, a 2025 study leveraged the Sustainable Development Science Satellite 1 (SDGSAT-1) to further enhance our understanding of health-integrated heat risk assessment for Karachi, Pakistan, and inform targeted interventions [11]. These studies evidence the ability to integrate GIS and remote-sensing techniques to visualize the HHR's spatial and temporal patterns as well as to identify its hotspots, i.e., areas where vulnerable populations are disproportionately affected by extreme heat events. Despite that, only a limited number of studies have undertaken long-term evaluations of HHR [20,21]. Further, they mostly have represented heat by means of air temperature, neglecting the effect of other physiologically relevant parameters on the human body, as it neglects other meteorological factors contributing to heat risk, such as humidity, air movement, and solar radiation [10].

Heat, in a human health context, is thermal energy transferred to the human body from the surrounding environment. Conditions of air temperature, humidity, wind speed, and radiation can be such that the heat transferred to the body is excessive [22]. This condition, called heat stress, may lead to heat stroke and dehydration and additionally trigger asthma attacks and respiratory and cardiovascular health diseases [23]. This combination of factors, along with the increased need for reliable evaluation methods of the outdoor environment [24], underscores the importance of studying human exposure to extreme heat rather than air temperature alone and developing effective heat mitigation strategies aimed at enhancing heat stress [10,25,26]. The Universal Thermal Climate Index (UTCI) is an internationally recognized human biometeorological indicator used to evaluate the connections between the outdoor environment, heat, and human well-being [27]. UTCI values are categorized into ten levels of thermal stress, ranging from "extreme cold stress" to "extreme heat stress" providing a comprehensive framework for evaluating thermal stress in various climatic conditions and increasing preparedness against extreme heat disasters [28].

To the best of our knowledge, there has been only one study that has incorporated heat, as per its proper definition, into the HHR assessment and used the UTCI for this purpose [6]. The study, however, was based on a heat stress–exposure–vulnerability framework and did not include hazard components. In contrast with traditional hazard indicators that directly measure external heat-related events such as heatwaves, the UTCI evaluates the effects of those events on human physiology by construction, and it does so by considering multiple factors that influence an individual's heat stress rather than evaluating the severity of a potential hazard. Therefore, it appears more suitable to use alongside other hazard–exposure–vulnerability indicators rather than as a standalone hazard indicator in the assessment of the heat risk to human health. The absence of a direct connection between HHR and thermal stress has resulted in a research gap, particularly in the accuracy and reliability of spatial and temporal patterns of the Heat Health Risk Indicator (HHRI) as a human health indicator during extreme heat events. This gap is further compounded by the significant lack of data on heat-related mortality and morbidity, making it challenging to understand and address the impacts of extreme heat fully.

In recent years, the Mediterranean region has emerged as a changing climate hotspot, with rising temperatures exceeding the global average rate [29]. Heatwaves have become more frequent, persistent, and deadly across the region [30]. Algeria, which has a 1200 km coastline along the Mediterranean Sea, has been listed by the IPCC as one of the vulnerable countries to climate change [31]. Every year, more than 260 people are estimated to die from heat-related illnesses in the country [32]. With annual temperatures predicted to increase by 2.5 to 3 °C and the temperature of the warmest month by 1.9 °C by 2100, prolonged exposure to extreme heat, which ultimately results in heat stress, is expected to occur at least once in the next five years with potentially deadly consequences [33]. On 26–28 April 2023, local temperatures in many regions in Algeria were up to 20 °C higher than the climatological average (1991–2020) for that time of year. This was made 100 times more likely by climate change, according to attribution studies [34].

Within this context, there is a clear need to consider environmental, social, and public health information and deploy it to develop effective, locally relevant climate-adaptive health solutions. Our paper responds to this need by deploying remote sensing, meteorological, and census data at the municipality level across 23 years (2001–2023). This research aims at (a) conducting a long-term spatio-temporal analysis (2001–2023) of the HHRI and the UTCI within an integrated hazard–exposure–vulnerability framework, (b) couple the HHRI with the UTCI to construct a comprehensive, multidimensional indicator that is able to enhance the understanding of heat-related health risks, and (c) identify and compare hotspots, i.e., areas that exhibit significant clustering of both high HHRI and the new coupled indicator values, particularly when these values are categorized as "high" or "very high". This research is the first in the Mediterranean context to assess HHR using the IPCC AR6 framework, providing a methodologically robust foundation for targeted adaptation plans and improved public health resilience in regions highly vulnerable to heat extremes.

2. Materials and Methods

The proposed methodology for the present research integrates hazard, exposure, and vulnerability components with the UTCI, a heat stress indicator that integrates air temperature (Ta), wind speed (V), vapor pressure (e), and the mean radiant temperature (Tmrt) to provide comprehensive spatio-temporal analysis and hotspot identification within the study area. The HHR assessment follows the framework defined by the IPCC's AR6 [4]. Data availability and previous studies guided the selection of these indicators. Table 1 presents each indicator, which either increases or lowers the HHR.

The methodology is divided into four main steps as outlined in Figure 1. It is designed to be reproducible, depending on open data published in a dataset repository to assure accuracy and transparency [35]. Moreover, the ArcGIS Pro 3.2.0 software [36] was used throughout the process to perform spatial analysis and visualization. We visualized maps by splitting the study period into four main intervals: (a) 2001–2006, (b) 2007–2011, (c) 2012–2016, and (d) 2017–2023.

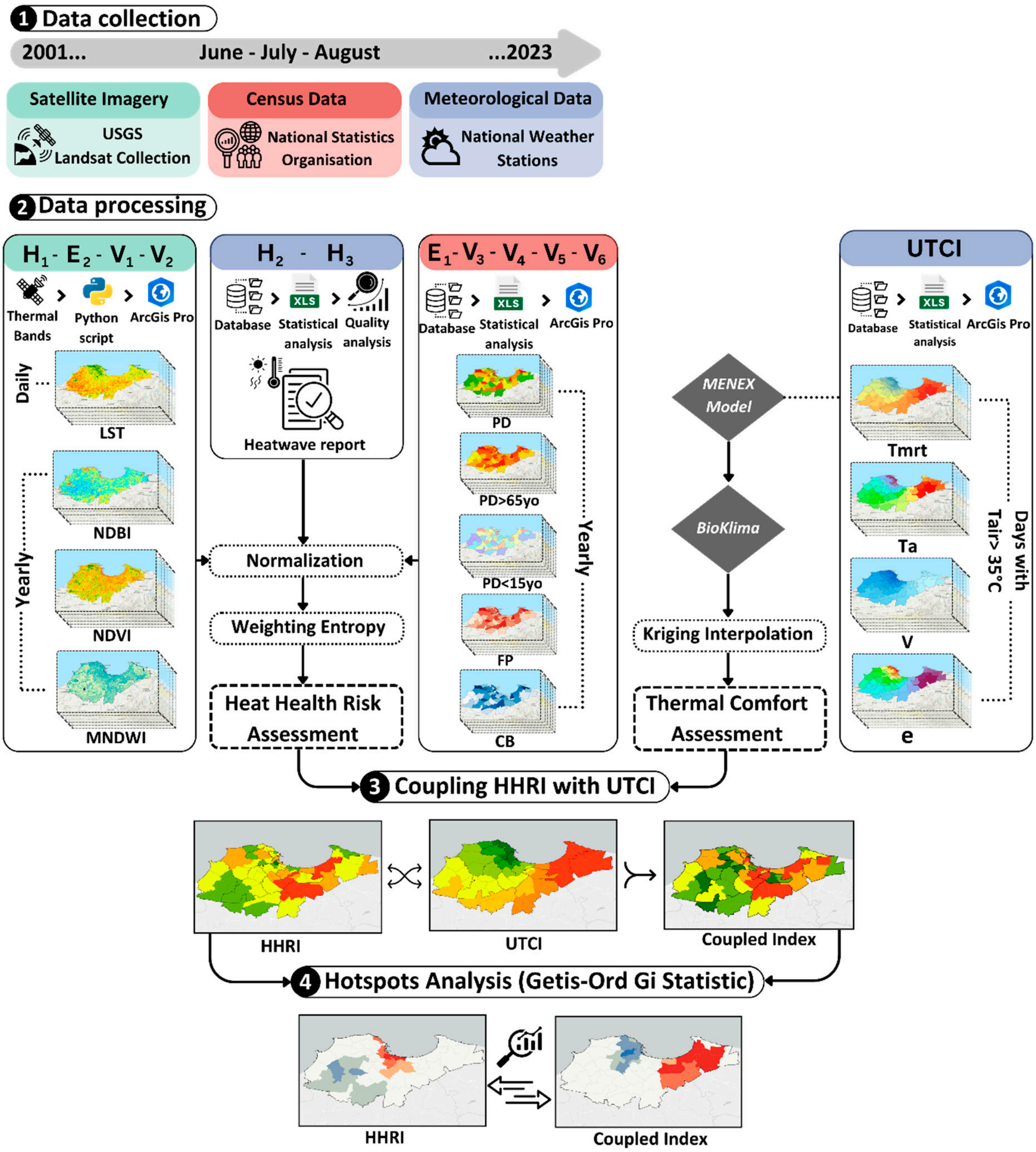

Figure 1. Study conceptual framework.

Table 1. Detailed description and calculation methods for each indicator used in the HHR assessment.

Category	Indicator	Description	Formula	Impact	References
Hazard	H1: LST Land surface temperature	The temperature of the Earth's surface is measured using satellite images of thermal bands	$LST = \frac{BT}{1+(w \times \rho BT) \times ln(\varepsilon)}$	(+)	[17,20,37]
	H2: Hot days	Days with maximum air temperatures greater than 35 °C	Count of days with Tair Max > 35 °C	(+)	[9,13,16]
	H3: Heatwave frequency	The number of events where the max daily average temperature exceeds 35 °C for more than 3 days	Count of days with Tair max > 35 °C for more than 3 consecutive days	(+)	[9,13,38]
Exposure	E1: (PD) Population density	Number of people per square kilometer	$\frac{Population}{Area}$	(+)	[15,37,38]
	E2: (NDBI) Normalized difference building index	An index used to measure built-up areas and urbanization	$\frac{(\text{SWIR}-\text{NIR})}{(\text{SWIR}+\text{NIR})}$	(+)	[39,40]
Vulnerability	V1: (NDVI) Normalized difference vegetation index	An index used to measure the density of vegetation	$\frac{(\text{NIR}-\text{Red})}{(\text{NIR}+\text{Red})}$	(−)	[37,40]
	V2: (MNDWI) Modified normalized difference water index	An index used to identify water bodies	$\frac{(\text{NIR}-\text{SWIR})}{(\text{NIR}+\text{SWIR})}$	(−)	[16,37,39]
	V3: (PD > 65 yo) Elderly population	The number of people aged 65 and older per square kilometer	$\frac{\text{Elderly population}}{Area}$	(+)	[14,16,18]
	V4: (PD < 15 yo) Young population	The number of people aged 15 and younger per square kilometer	$\frac{\text{Young population}}{Area}$	(+)	[14,17,41]
	V5: (FP) Female population	Number of females per square kilometer	$\frac{\text{Female population}}{Area}$	(+)	[6,15,39,42]
	V6: (CB) Care beds	The number of available care beds available per municipality	Total Care Beds per municipality	(−)	[6,9,15]

SWIR: reflectance in the shortwave infrared band; NIR: reflectance in the near-infrared band; Red: reflectance in the red visible band.

The indicators (H1, H2, H3, E1, E2, V1, V2, V3, V4, V5, V6) are detailed in Table 1.

2.1. Data Collection

The study focuses on Algiers, the capital of Algeria, situated at 36°46′34″ N and 3°03′36″ E (Figure 2). With its 80 km coastline along the Mediterranean Sea and varied topography, Algiers has a Mediterranean climate (Csa) according to the Köppen climate classification. It typically has long, hot, and dry summers, with average daily maximum temperatures exceeding 30 °C, heatwaves occasionally pushing temperatures above 35 °C, and minimal to no precipitation. Considering it is the most densely populated province in Algeria, with an estimated population of 3,309,896 divided into 57 municipalities according to the 2020 statistical yearbook, it serves as a great case study for assessing heat health concerns and heat stress.

Three types of data were used in the study: satellite, meteorological and census data.

Satellite data were obtained from the United States Geological Survey (USGS) [43] during March and April 2024, leveraging Landsat Collection 2. The data covered a series of sensors across different Landsat missions, specifically Landsat 5 Thematic Mapper (TM), Landsat 7 Enhanced Thematic Mapper Plus (ETM+), and Landsat 8/9 Operational Land Imager and Thermal Infrared Sensor (OLI/TIRS). Scenes with a cloud cover of 5% or less were selected, with a spatial resolution of 30 m. The temporal resolution of the dataset spans the summer months of June, July, and August from 2001 to 2023. The associated Metadata (MTL) files were used to perform atmospheric corrections, ensuring the accuracy of derived hazard, exposure, and vulnerability indices, namely the LST, normalized difference building index (NDBI), normalized difference vegetation index (NDVI), and modified normalized difference water index (MNDWI).

Meteorological data were acquired from four national weather stations within the study area, covering the same study period (summer months from 2001 to 2023). The data include hourly air temperature, relative humidity, and wind speed parameters. This meteorological dataset is required to calculate the UTCI [27] and the hazard components of the HHRI (hot days and heatwave frequency).

Census data were obtained from the statistical yearbook established by the National Statistical Organization for the study area from 2001 to 2023. This dataset covers population density, population under 15 and above 65, female population, and the number of available public care beds in each municipality to measure both exposure and vulnerability components.

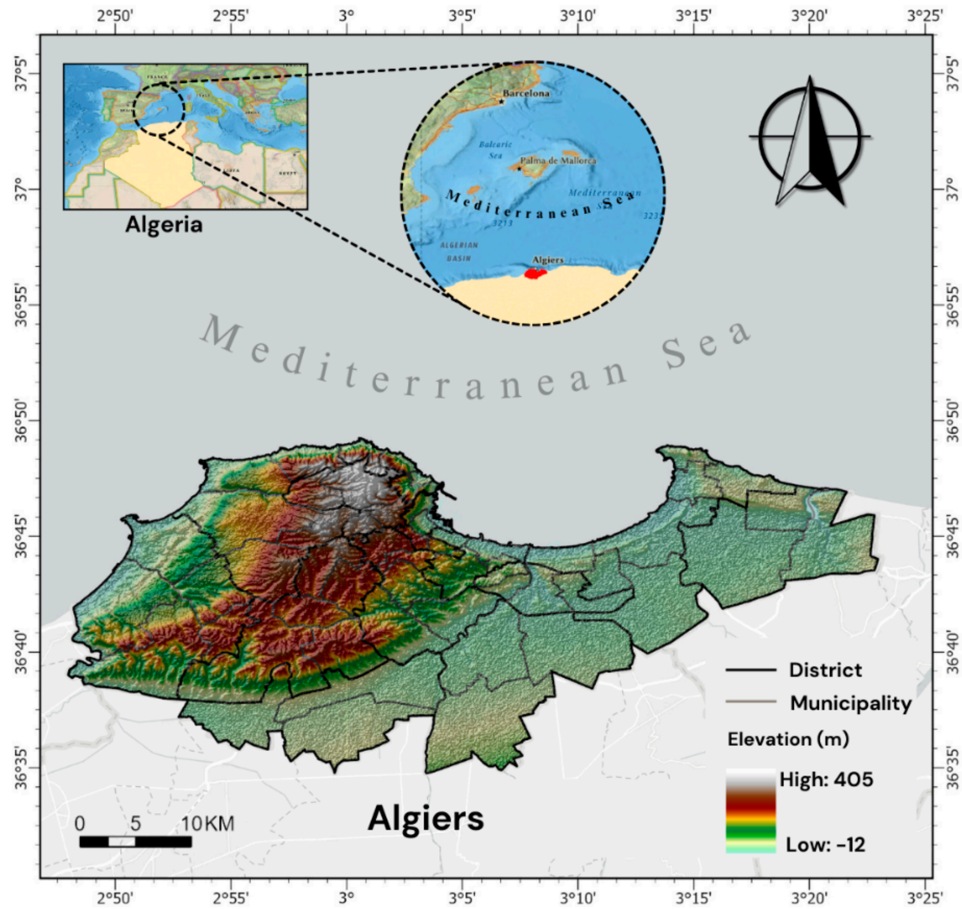

Figure 2. Study area location and elevation map.

2.2. Data Processing

2.2.1. Heat Health Risk Assessment

The spatial and temporal resolution of the collected data provided a solid foundation for our investigation, allowing comprehensive analysis and mapping of the indicators, and ensuring accurate spatial representation. The assessment of heat hazards included LST (H1) to quantify the surface-level heat intensity that directly impacts the HHR [44], as well as hot days (H2) and heatwave frequency (H3) to highlight prolonged periods of extreme heat that can increase the HHR [45]. Population density (E1) was selected for its high concentration of at-risk individuals, while NDBI (E2) reflects built-up areas' contribution to heat risk [46]. Vulnerability assessment included NDVI (V1) and MNDWI (V2) as positive indicators, as vegetation and water bodies help to reduce thermal stress [47]. The elderly population (V3) and young population (V4) were negative indicators due to their higher sensitivity to heat-related illnesses [42,48]. The female population (V5) was included due to potential gender disparities in heat tolerance [49]. Care beds (V6) were a positive indicator, reflecting healthcare capacity to handle HHR emergencies.

Satellite data were used to compute four key indicators (H1, E1, V2, V3) with atmospheric corrections. Python scripts in ArcGIS Pro 3.2.0 generated 148 daily LST maps, with 43% linked to heatwaves. Annual NDBI, NDVI, and MNDWI averages produced 23 maps per indicator (2001–2023). Meteorological analysis identified 770 hot days and 23 heatwave events, while census data provided municipality-level maps of population, age groups, female ratio, and care beds.

Because the HHR assessment integrates multiple environmental and demographic indicators, each with different units, the indicators were normalized to a common scale using the Min–Max normalization method to guarantee that each indicator contributes equally to the final index by bringing all variables to a uniform scale based on Equation (1):

$$\text{Xnorm} \begin{cases} = \frac{\text{X}-\text{Xmin}}{\text{Xmax}-\text{Xmin}} \; (for\ positive\ indicators) \\ = \frac{\text{Xmax}-\text{X}}{\text{Xmax}-\text{Xmin}} \; (for\ negative\ indicators) \end{cases} \tag{1}$$

where Xnorm is the normalized value, X is the original value, Xmin is the minimum value, and Xmax is the maximum value.

Next, the entropy weighting approach was performed to assign weights to each indicator based on their variability and contribution to heat risk. This approach was used in several studies in the HHR assessment [39,50] and includes four main steps as presented in Figure 3.

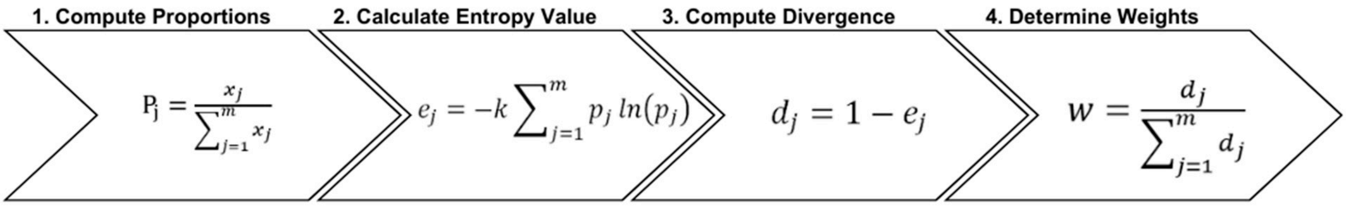

Figure 3. Entropy weighting process for indicator weight calculation.

Where Pj is the proportion of the normalized indicator, ej is the entropy value of the indicator j, dj is the degree of diversification for the indicator j, Wj is the weight assigned to the indicator j, xj is the normalized value of the indicator j, m is the total number of indicators, and K is a constant defined as 1/ln (m).

These indicators were then combined into a single index and finally mapped to visualize the overall HHRI using the Crichton risk triangle equation shown in Equation (2), and the levels of risk were then divided into five classes from "very high" to "very low" using the natural breaks (Jenks) option in ArcGIS Pro:

$$\text{HHRI} = \text{H} \times \text{E} \times \text{V} \tag{2}$$

where Hrepresents hazard, E represents exposure, and V represents vulnerability.

2.2.2. Heat Stress Assessment

Unlike simpler indices, UTCI integrates factors such as air temperature (Ta, °C), wind speed (V, m/s), vapor pressure (e, hPa), and the mean radiant temperature (Tmrt, °C), to provide a detailed understanding of thermal stress on the human body [51]. UTCI is expressed in terms of an assessment scale, which is composed of ten stress categories. Each category represents specific physiological and thermoregulatory responses to environmental conditions [52]. As this study focuses on the summer season, five stress levels ranging from no thermal stress to extreme heat stress were considered (Table 2).

Table 2. UTCI heat stress assessment scale (adapted from Bröde et al., 2012 [27]).

UTCI (°C)	Stress Category
UTCI $\geq$ 46	Extreme heat stress
38 $\leq$ UTCI < 46	Very strong heat stress
32 $\leq$ UTCI < 38	Strong heat stress
26 $\leq$ UTCI < 32	Moderate heat stress
9 $\leq$ UTCI < 26	No thermal stress

Daytime meteorological parameters (from 6:00 am to 6:00 pm) were extracted for each day within the study period. The kriging interpolation tool was used to represent the spatial distribution of these parameters across the study area. The UTCI was calculated for hot days, defined as days when the air temperature exceeded 35 °C, in order to better capture the extreme heat risk conditions which typically occurred between 1:00 pm and 3:00 pm, to better reflect peak thermal stress periods and avoid underestimation due to lower morning values. This same time window was applied consistently across all input parameters used in the UTCI computation. Additionally, wind speed measurements were adjusted from 10 m to 1.2 m using the logarithmic wind profile equation (Equation (3)):

$$v(z) = v_{\text{ref}} \frac{\ln(z/z_0)}{\ln(z_{\text{ref}}/z_0)} \tag{3}$$

where $v(z)$ is the wind speed at 1.2 m, $v(z_{\text{ref}})$ is the measured wind speed at the reference height, z is the target height, z_{ref} is the reference height, and z_0 is the surface roughness length.

The UTCI was calculated using the collected data and the Tmrt via the operational procedure by [27]. The calculation of UTCI was carried out by the software package BioKlima 2.6 [53] using Equation (4):

$$\text{UTCI} = \text{Ta} + \text{Offset (Ta,V,e,Tmrt)} \tag{4}$$

The MENEX model [54] was used to calculate Tmrt [6,55], through Equations (5)–(8):

$$\text{Tmrt} = \left[(\text{Rprim} + 0.5\text{Lg} + 0.5\text{La}) / \left(0.95 \times 5.667 \times 10^{-8}\right)\right]^{1/4} - 273.16 \tag{5}$$

$$\text{La} = 5.5 \times 10^{-8}(273.16 + \text{Ta})^4 \left[0.82 - 0.25 \times 10^{-0.094 \times 0.75\text{e}}\right] \tag{6}$$

$$\text{Lg} = 5.5 \times 10^{-8}(273.16 + \text{Tg})^4 \tag{7}$$

$$\text{Rprim} = 1.4[-100.428 + 73.981\ln(\text{h})](1 - 0.01\text{a}_\text{c})\text{Irc} \tag{8}$$

where La and Lg represent the longwave radiation emitted by the air and the ground, respectively, both measured in (W/m^2); Tg refers to LST (°C); Rprim (W/m^2) represents the absorbed solar radiation; the terms h and a_c denote the sun altitude (degree) and albedo of skin (%), respectively; and Irc represents the reduction coefficient of heat transfer through clothing.

2.3. Coupling HHRI and UTCI

The major step in our methodology involves the coupling of the HHRI with the UTCI to provide a comprehensive view of heat-related risks and thermal stress in Algiers. This process integrates the spatial distributions of both indicators to identify areas experiencing the highest combined risk. To achieve this, both the HHRI and UTCI values were then normalized to a common scale (0–1) to ensure compatibility and comparability, as well as the integration of the two indicators into a single map. The normalization was performed using the Min–Max normalization method expressed in Equation (1). The normalized HHRI and UTCI were then coupled using the raster calculator tool in ArcGIS Pro 3.2.0 software following Equation (9):

$$\text{Coupled Index} = \frac{\text{HHRI} + \text{UTCI}}{2} \tag{9}$$

We used equal weights to ensure that both HHRI and the UTCI contribute equally to the combined risk assessment. The resulting coupled index was then mapped to provide a visual representation of areas where high HHRI and high UTCI values intersected.

2.4. Hotspots Analysis (Getis-Ord Gi*)

The final step of our methodology aimed at identifying spatial clusters of extreme risk areas within the study area. To further refine our understanding, Getis-Ord Gi*—a spatial analysis tool that identifies areas of significant clustering, including those that are most vulnerable to risk [56]—was applied to both the HHRI and the coupled index maps. The analysis identifies both hot and cold spots, which are areas of statistically significant clustering of "very high" and "high" or "very low" and "low" values. They were classified into seven categories: cold spot with 99% confidence, cold spot with 95% confidence, cold spot with 90% confidence, not significant, hotspot with 99% confidence, hotspot with 95% confidence, and hotspot with 90% confidence. By identifying hotspots of both HHRI and the new coupled index, we created detailed maps highlighting the areas that require targeted interventions to heat stress, considering both HHR risk and thermal stress.

3. Results

The results are structured into four sections: (1) HHR assessment, covering hazard, exposure, vulnerability, and HHRI; (2) UTCI analysis; (3) the coupled HHRI–UTCI index; (4) hotspot analysis for refined risk evaluation. The study spans four periods, (a) 2001–2006, (b) 2007–2012, (c) 2013–2018, and (d) 2019–2023, presented at the municipal level in Algiers (57 municipalities).

3.1. Heat Health Risk Assessment

3.1.1. Hazard Index

Figure 4 shows the spatial distribution of the hazard index. Throughout (a), the hazard index mainly ranged from "moderate" to "very high", with 58% of total municipalities (e.g., Shaoula). Moving to (b), the extent of "very high" areas expanded to 19% in the southern districts (e.g., Birtouta). In contrast, in (c) there was a consistent expansion in the hazard index in the eastern regions (e.g., Dar El Beida). Finally, (d) indicates a continuation of these patterns, with 39% of areas classified as "high" and "very high" due to the rising LST values there.

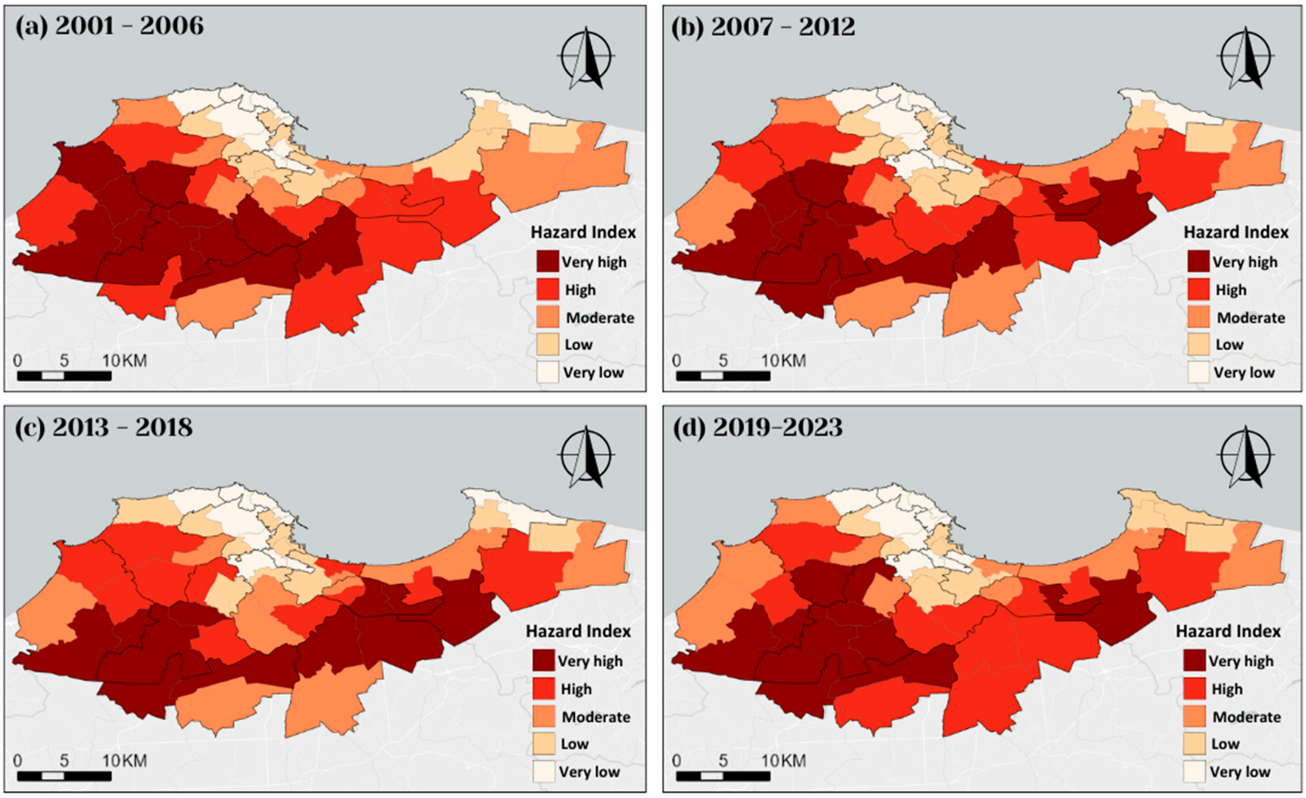

Figure 4. Spatial distributions of the hazard index in Algiers. (**a**) 2001–2006, (**b**) 2007–2012, (**c**) 2013–2018, (**d**) 2019–2023.

3.1.2. Exposure Index

Figure 5 illustrates the spatial distribution of the exposure index. In (a) and (b), 30% of the total municipalities had the highest levels of exposure, classified as "high" and "very high", mainly in the north (e.g., The Casbah), while 50% experienced "very low" levels (e.g., Mahelma). In (c), there was a further expansion of "high" levels, with 26% of municipalities identified in the central regions (e.g., El Achour). This trend continued, with "very low" levels nearly disappearing in (d) with only 11% of the total municipalities. At the same time, new areas were categorized as "high" and "very high" (e.g., Mahelma and Baba Hassen) due to increasing population and urbanization in the last 10 years in those areas.

3.1.3. Vulnerability Index

Figure 6 demonstrates the spatial distribution of the vulnerability index. In (a), "very high" levels were dispersed across 12% of the total municipalities in the central and eastern regions (e.g., Bordj El Kiffan). In contrast, "low" and "very low" levels were primarily found in the southern municipalities (e.g., Zeralda) with 35%. In (b), although vulnerability levels increased and "very low" areas nearly disappeared, the proportion of "very high" municipalities decreased to 8%, which is lower than in the previous period. However, (c) showed a shift in the spatial pattern, with lower vulnerability levels in the central districts (e.g., Shaoula). Finally, in (d), the pattern was similar to (c), but with only 5% of areas classified as at the "very high" vulnerability level and only one municipality (Sidi M'hamed) at the "very low" level. The increase in vulnerability over time is likely due to the growing population of vulnerable groups, such as the elderly and young, which intensifies the overall risk.

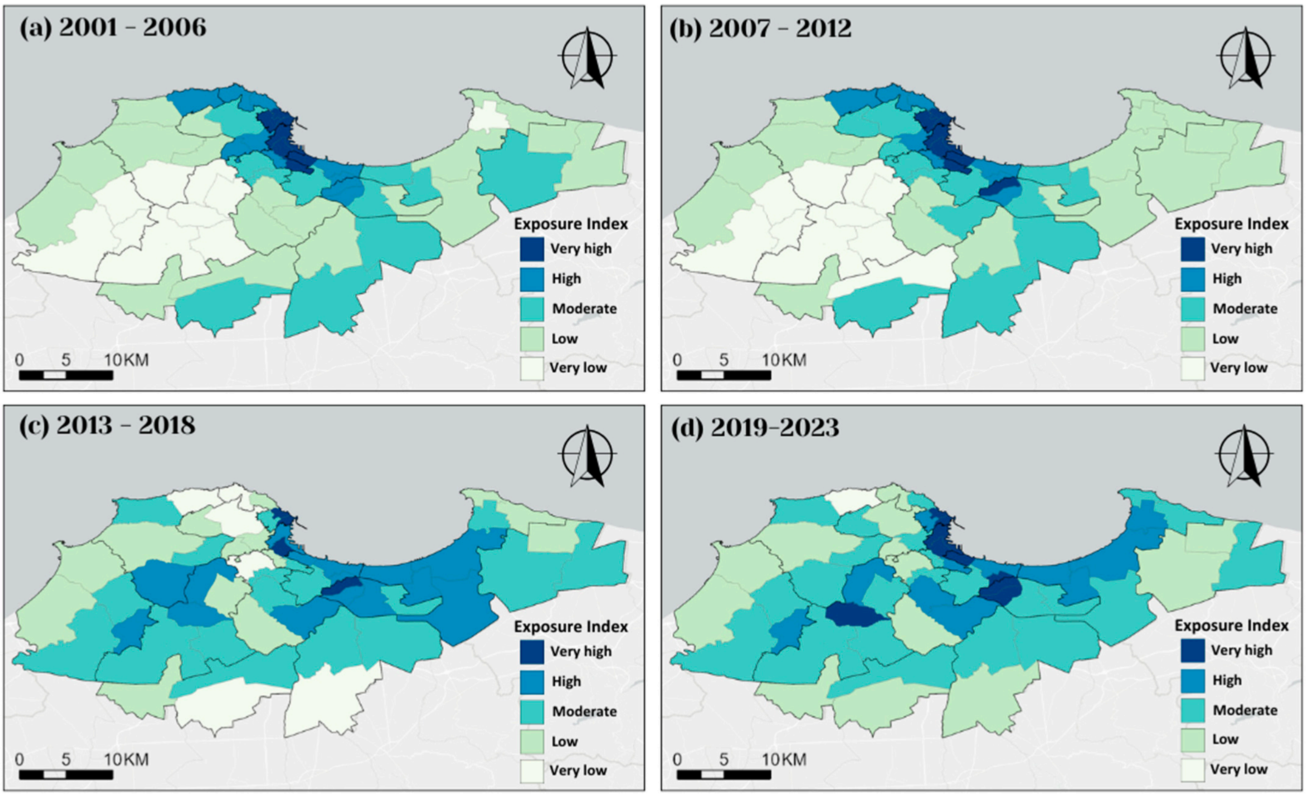

Figure 5. Spatial distributions of the exposure index in Algiers. (**a**) 2001–2006, (**b**) 2007–2012, (**c**) 2013–2018, (**d**) 2019–2023.

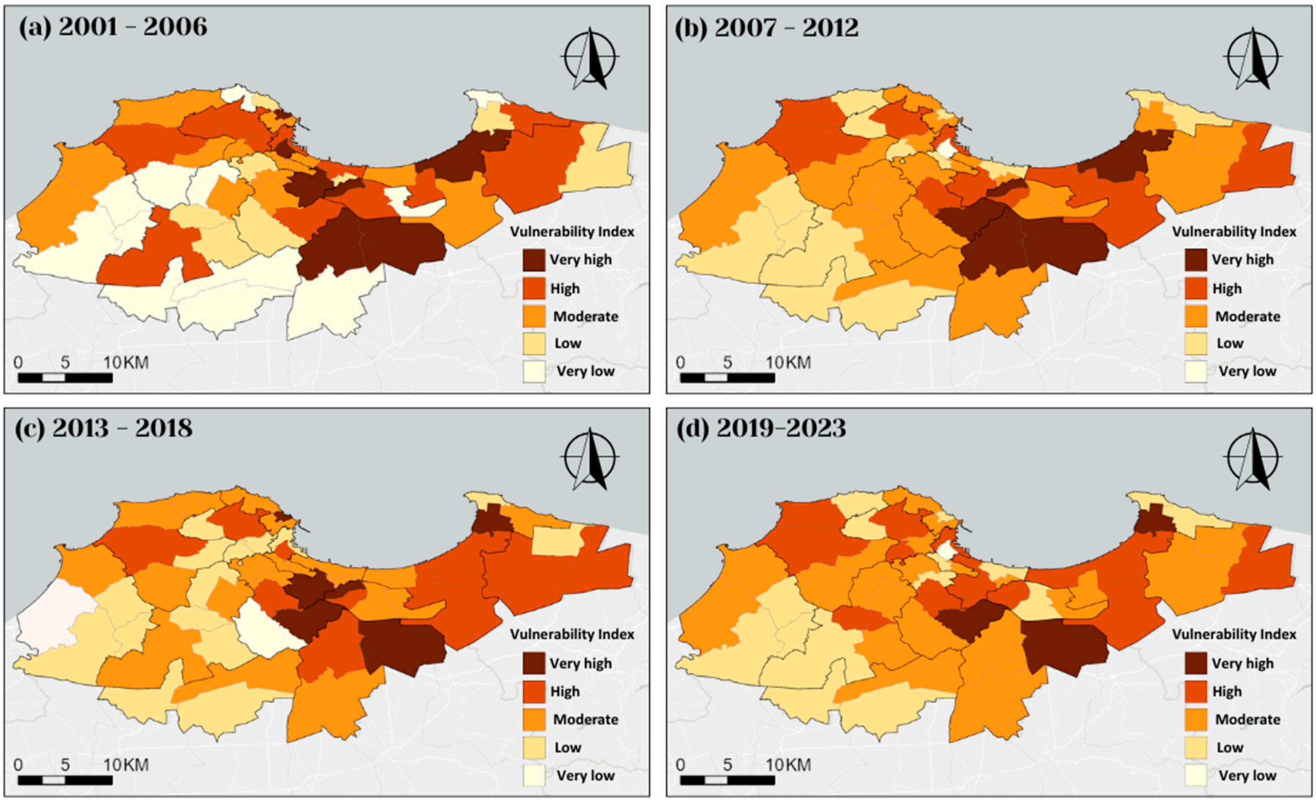

Figure 6. Spatial distributions of the vulnerability index in Algiers. (**a**) 2001–2006, (**b**) 2007–2012, (**c**) 2013–2018, (**d**) 2019–2023.

3.1.4. Heat Health Risk Index (HHRI)

Figure 7 demonstrates the spatial distribution of the HHRI. In (a), the HHRI was higher in the central regions as well as several scattered municipalities in both the east and west, with 18% of municipalities identified as "very high" risk and 19% as "high". However, "moderate" risk was more common, with 28% of municipalities across the province. The areas with a majority of "low" and "very low" risk tended to be in the southern and western parts (e.g., Birtouta). Moving into (b), an increase in HHRI intensity was observed across the province, with areas that were classified as having "low" and "very low" risk levels increasing to "moderate" risk in nearly half of the total municipalities (e.g., Draria); however, the "very high" risk level identified municipalities slightly decreased to 11%. Algiers witnessed a decrease in HHRI intensity throughout period (c), with only two municipalities remaining in the "very high" risk category (Bab El Oued and Bachedjerah). Both "high" and "moderate" risks reduced equally, while "low" risk levels remained unchanged, and "very low" levels were identified in only one single municipality (Shaoula). Lastly, (d) exhibited a rise in intensity, as some central municipalities (e.g., Kouba) experienced a shift from "moderate" to "high" risk, and 7% of municipalities (e.g., Eucalyptus) reverted to the "very high" category. The changes in risk levels over time highlight the varying degrees of resilience and vulnerability within different municipalities, particularly in the central regions where persistent high-risk areas reflect ongoing challenges in managing HHR.

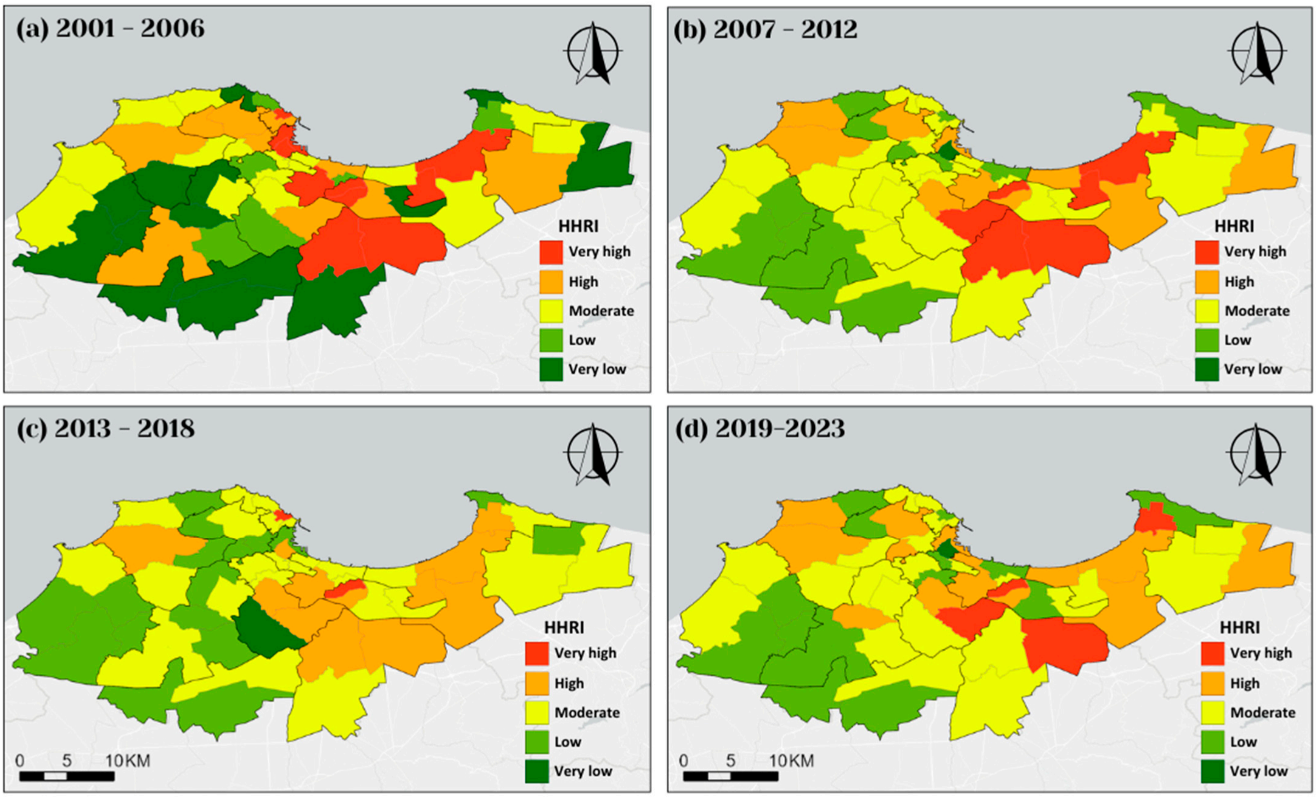

Figure 7. Spatial distributions of HHRI in Algiers. (**a**) 2001–2006, (**b**) 2007–2012, (**c**) 2013–2018, (**d**) 2019–2023.

3.2. Universal Thermal Climate Index (UTCI)

The UTCI maps (Figure 8) illustrate the spatial distribution of thermal stress across the study area, identifying regions experiencing varying levels of heat stress over the four distinct periods. In (a), UTCI values ranged from 24.1 °C to 32.0 °C, with the majority of areas in the "moderate heat stress" category. Notably, the highest levels of thermal stress were concentrated in the eastern and southern municipalities (e.g., Ain Taya). In contrast, the western and northern ones (e.g., Rais Hamidou) exhibited more favorable conditions, falling within the "no thermal stress" to "moderate heat stress" categories. The thermal stress further intensified in (b), with the highest values reaching 37.0 °C. This shift places the central and eastern regions (e.g., Oued Smar) into the "strong heat stress" category. At the same time, the northern areas (e.g., El Biar) continued to experience lower stress levels, mostly within the "moderate heat stress" range. In (c), the thermal stress decreased slightly, with the highest UTCI recorded at 36.1 °C, maintaining most of the area inside the "strong heat stress" category. However, the central regions (e.g., Sidi M'hamed) exhibited a slight decrease in stress. In contrast, the northern regions (e.g., Oued Koriche) continued to benefit from comparatively thermally favorable conditions, with the lowest UTCI recorded at 28.8 °C, inserting them in the "moderate heat stress" category. Lastly, (d) experienced a small rise in thermal stress, with the highest UTCI value identified during the four periods rising to 38.1 °C and with a minimum temperature of 29.3 °C, reaching the "very strong heat stress" category. Despite these moderate shifts, the overall trend of thermal stress across the study area and for all four periods remained stable, with the northern areas constantly experiencing lower stress levels compared to the central and eastern ones.

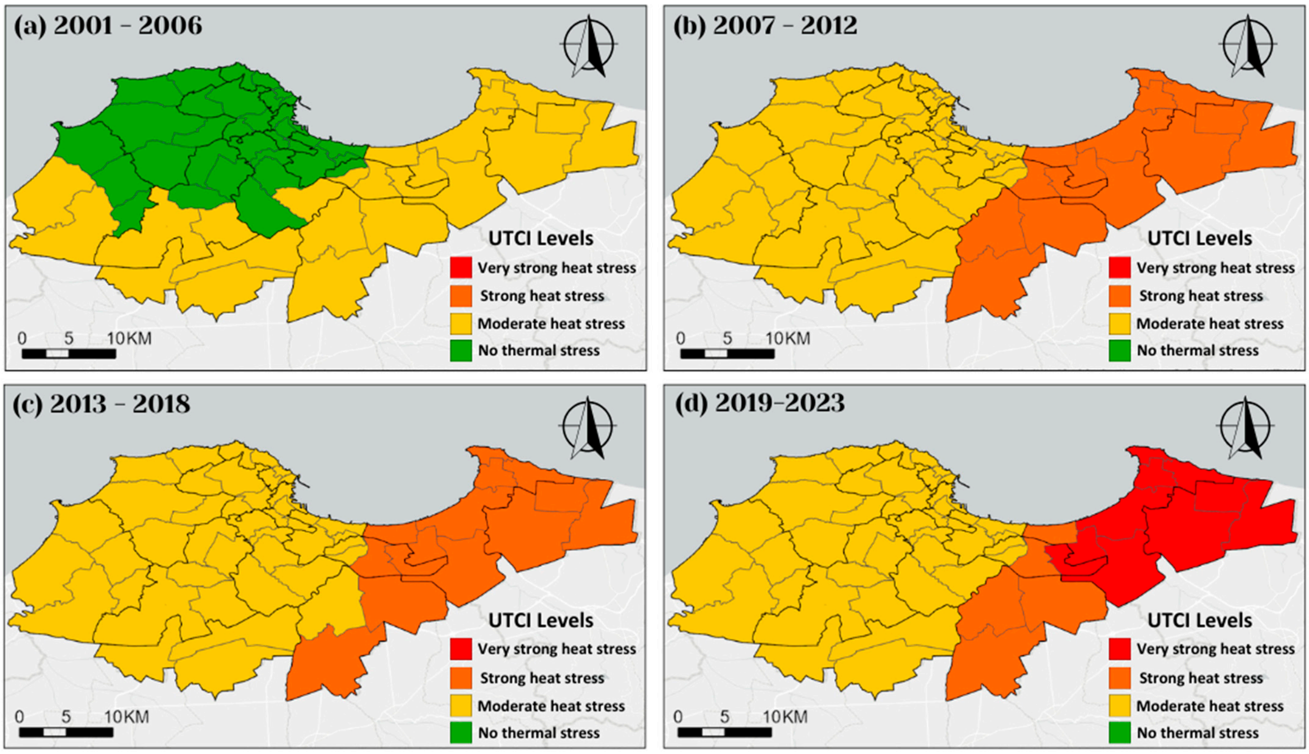

Figure 8. Spatial distributions of UTCI in Algiers. (**a**) 2001–2006, (**b**) 2007–2012, (**c**) 2013–2018, (**d**) 2019–2023.

3.3. Coupled Index

The coupling of the HHRI with the UTCI indicates considerable variations in risk throughout the study area and during the four periods (Figure 9). In (a), the combined index was higher in the eastern regions (e.g., Rouiba) compared to other municipalities, with 7% of them classified as "very high" risk and 14% as "high." The "moderate" risk level was identified in a few scattered municipalities (e.g., Kouba) across the province. However, "low" and "very low" levels were more common across the study area, with 37% and 25% of municipalities (e.g., Ouled Chbel and Sidi Moussa), respectively. Moving into (b), the intensity of the combined index increased to 42% of municipalities under "high" and "very high" levels in the central, eastern, and western regions of the city (e.g., Kouba and Heraoua). Moreover, fewer "low" and "very low" risk areas (42%) were identified in the south (e.g., Souidania). A continuing escalation in intensity was observed throughout (c), with just one municipality (Saoula) remaining in the "very low" risk category. However, the "moderate" risk level saw an increase, with almost half of the total municipalities spread across the study area in a disconnected pattern, and only 7% of total municipalities (e.g., Bab Ezzouar) identified in the "very high" category. Finally, (d) saw a spike in intensity, as the majority (47%) of central municipalities shifted from "low" to "moderate" levels (e.g., Dely Brahim). In comparison, the "very low" level was maintained in only 5% of municipalities. Despite this increase, some municipalities (e.g., Bab Ezzouar) shifted from the "moderate" to the "high" risk category, demonstrating some overall instability in the broader region.

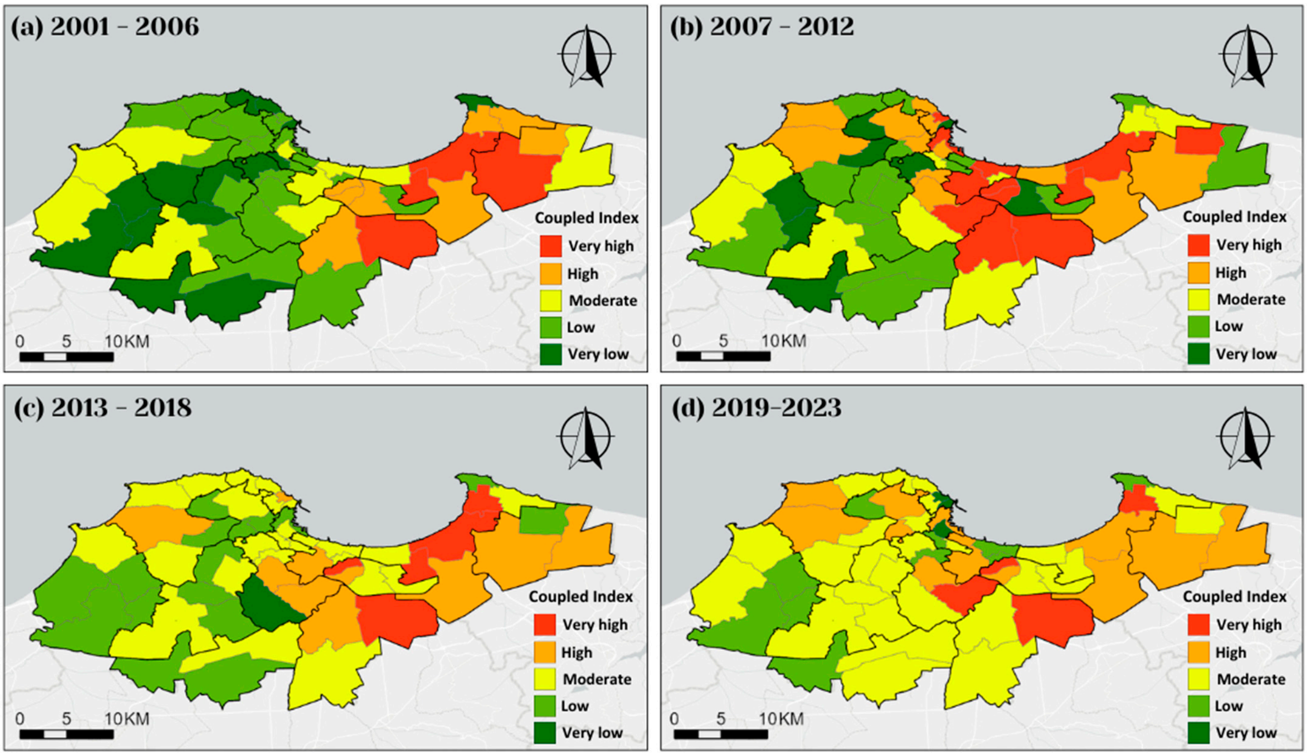

Figure 9. Spatial distributions of the coupled index in Algiers. (**a**) 2001–2006, (**b**) 2007–2012, (**c**) 2013–2018, (**d**) 2019–2023.

The coupling of the HHRI and UTCI provided an improved understanding of the spatial and temporal dynamics of heat health risks in Algiers. The variations in risk levels recorded across different periods reflect the evolving interplay between heat stress and population vulnerability. This pattern notably highlights the increased risks in the central and eastern regions, which may be influenced by factors such as urban density and demographic composition.

3.4. Hotspots Analysis

Figure 10 represents the spatial distribution of the HHRI hotspots (a, b, c, d) and the coupled index hotspots (a′, b′, c′, d′) over the four study periods using the Getis-Ord Gi* statistical method resulting in three levels for both hotspots and cold spots along with a not-significant area.

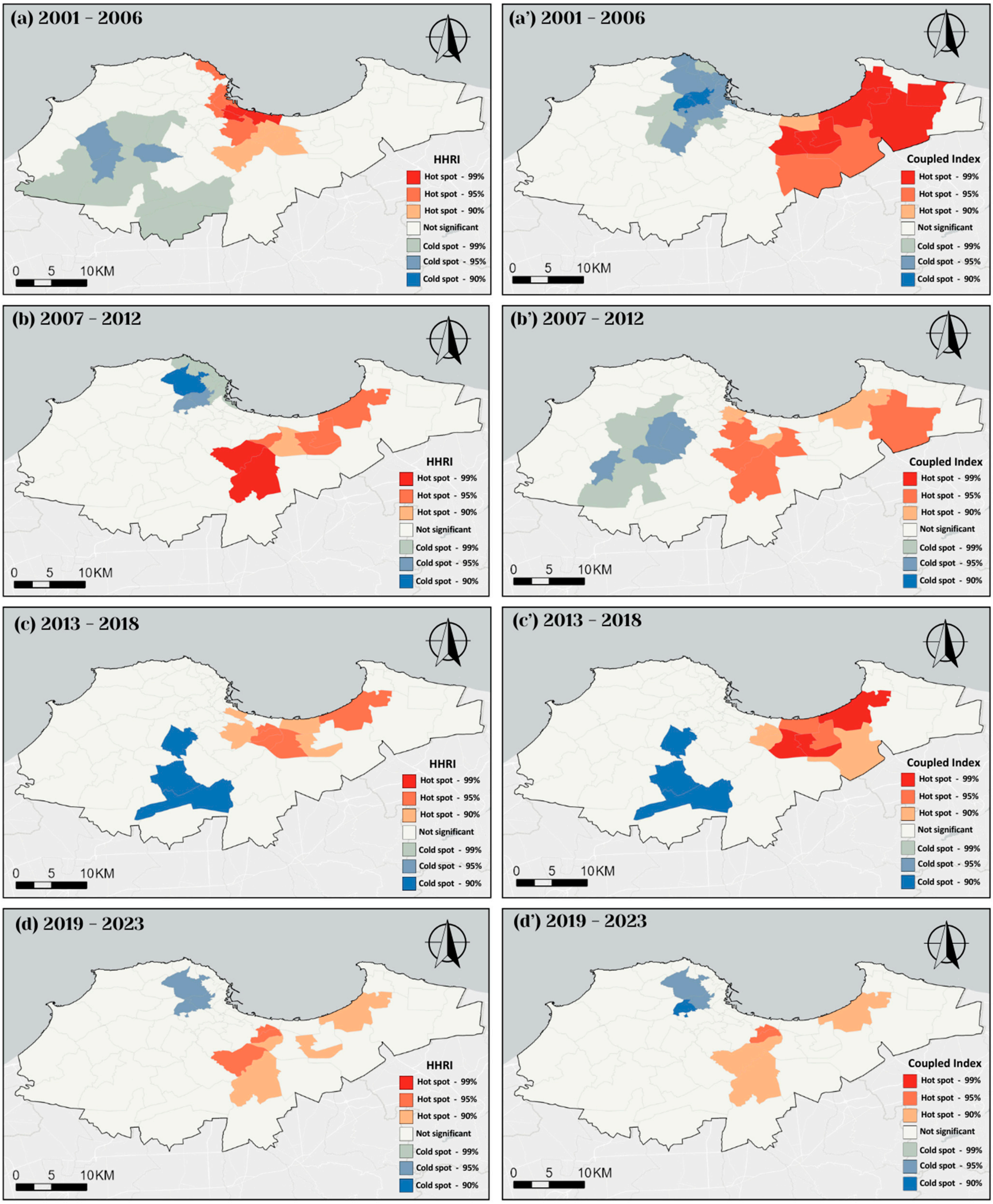

Figure 10. Spatial distributions of HHRI hotspots and cold spots in Algiers. (**a**) 2001–2006, (**b**) 2007–2012, (**c**) 2013–2018, (**d**) 2019–2023. Spatial distributions of the coupled index hotspots and cold spots in Algiers. (**a'**) 2001–2006, (**b'**) 2007–2012, (**c'**) 2013–2018, (**d'**) 2019–2023.

In the first period, HHRI hotspots were identified primarily in the extreme northern and eastern regions, as shown in (a), with 1.18% of the total area classified as a hotspot with 99% confidence. Most of the regions (66.5%) were not significant, and no cold spot with 99% confidence was identified, while 21% of the total area was classified as a cold spot with 95% confidence. Alternatively, (a′) shows a significantly larger area (14.22%) under the hotspot category at 99% confidence in the coupled index, mainly in the eastern regions. This suggests a broader risk when human thermal stress is integrated, as shown in Figure 11, while the cold spot area was smaller compared to the HHRI, at 3.4% with 99% confidence.

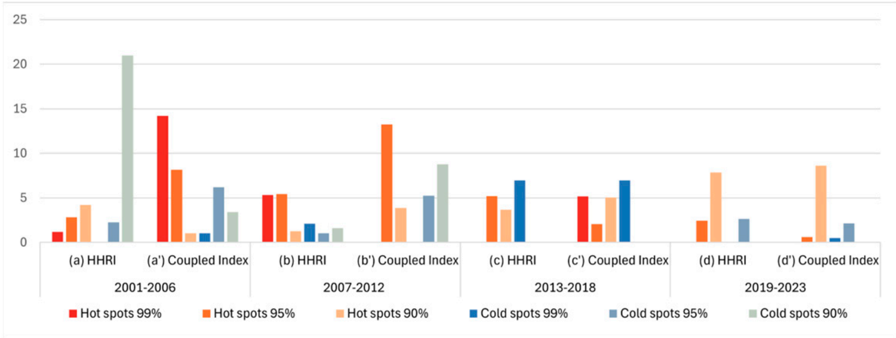

Figure 11. Temporal analysis of hotspots and cold spots in the HHRI and the coupled index in Algiers municipalities (2001–2023).

During the second period, both the intensity and spatial distribution of the HHRI and coupled index hotspots changed. As shown in (b), HHRI hotspots with 99% confidence increased to 5.3% of the total area, with concentration in the central regions, alongside a notable rise in "not significant" areas, reaching 83.3%. Cold spots decreased to 2.09% with 99% confidence, primarily in the northwestern regions. In contrast, (b′) shows a decrease in coupled index hotspot intensity, with no area classified at 99% confidence but 13.23% at 95% confidence, mostly in the eastern and central regions. The "not significant" areas remained constant compared to the previous period. At the same time, cold spots decreased to 5.23% at 95% confidence in the central to western regions, with no cold spots at 99% confidence, as observed in Figure 11.

The third period went through another shift in both indicators, with practically the same distribution across the study area. Figure 10c reveals a large drop in HHRI hotspots, with no areas categorized at 99% confidence and only 5.2% of the total area categorized at 95% confidence in eastern regions, while cold spots increased to 6.98% at 99% confidence in the south, leaving most of the city categorized as "not significant" area with 84.1%. Moreover, (c″) shows coupled index hotspots with 5.17% at 99% confidence in the eastern regions once again, while it shares the same cold spot intensity and distribution with the HHRI as shown in Figure 11.

Finally, there was a further change for both indicators in the fourth period, although with a different intensity but the same spatial pattern. Figure 10d indicates a shift of HHRI hotspots from the extreme north to the central regions, with no areas categorized at 99% confidence, while 2.46% of the total area was categorized at 95% confidence. Furthermore, cold spots experienced an entire migration towards northern regions with just 2.62% at 95% confidence. The combined index hotspots, however, decreased to only one municipality in the east and a few other ones in the central region with only 0.62% at 95% confidence as indicated in (d′). At the same time, there were no hotspots categorized at 99% confidence. Cold spots classified at 99% confidence were identified within a smaller area with just 0.48%, while a "not significant" area remained dominant with 88.1% as summarized in Figure 11.

Pearson correlation analysis was conducted for both indicators of cold/hotspots across the four periods (Figure 12). The *p*-value increased from −0.25 in the first period to 0.96 in the last period, highlighting how linked environmental, urban dynamics, and demographic factors are in increasing heat risk. This upward trend indicates a strengthening relationship between the distribution of hotspots and the underlying risk components, supporting the spatial patterns observed in the HHRI analysis.

Figure 12. Matrix of the Pearson correlation coefficients between the HHRI and the coupled index (2001–2023).

Throughout the study period, persistent hotspots (Figure 13) were identified in Bordj El Kiffan, El Harrach, and Bourouba, while consistent cold spots were observed in Draria, Bouzareah, and Ben Aknoun.

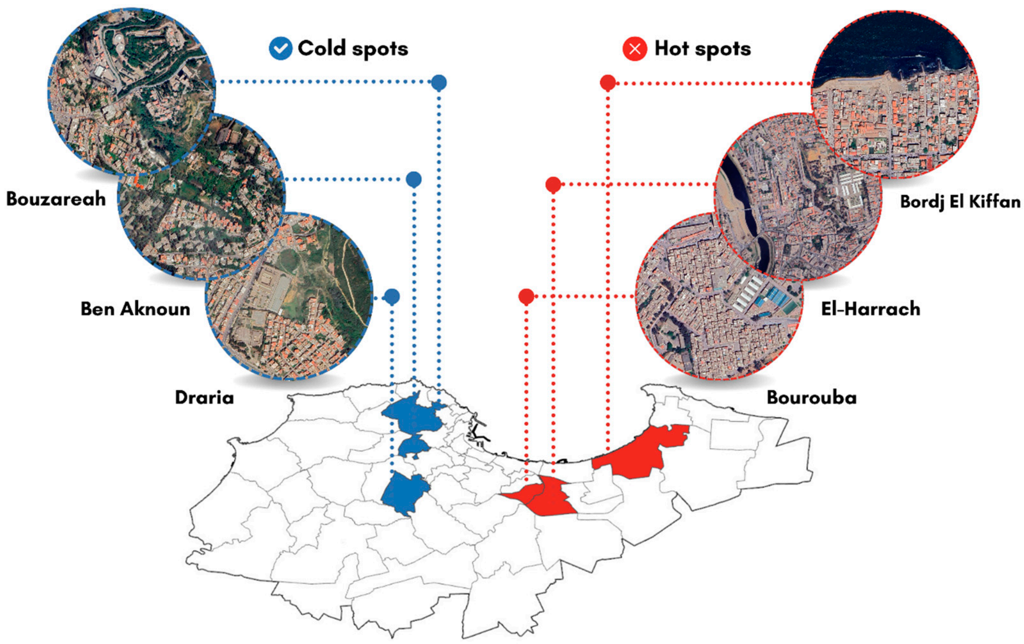

Figure 13. Persistent hotspots and cold spots of the coupled index in Algiers (2001–2023).

4. Discussion

4.1. HHR Assessment

To our knowledge, this paper is the first to assess HHR in Algiers and, more broadly, the first to undertake a long-term multi-decade (2001–2023) analysis of HHRI in any Mediterranean, African, or MENA country. While there is limited prior research in this area, one previous study has conducted a long-term HHR assessment, although in a different climatic context [20]; another study focused on a shorter timeframe [17]; and several others have examined HHRI during summer days and months [8,15,19], as well as during heatwave periods [6,12]. Our HHR assessment framework followed the IPCC AR6 employing the three risk components, hazard, exposure, and vulnerability, as defined from decades-spanning satellite imagery, census data, and meteorological data.

Our findings reveal that the intensity of HHRI has increased over time, since "very-low" risk areas had an outstanding decrease (93%) and almost disappeared—likely due to the global and regional climate change in rising temperatures and the frequency of extreme heat events [57]. Moreover, Algiers had a massive and rapid urbanization with a substantial increase (113.67%) in built-up areas from 1995 to 2023 [58]. People from all over the country are looking for better life conditions in the capital, leading to a massive expansion of built-up areas. Our analysis also suggests that the shifts in HHRI hotspots are due to changes in land use and the development of new infrastructure areas that were once less developed and urbanized, causing higher risk levels [59].

However, our results differ from previous studies that identified the most populated areas as the highest risk for heat-related health issues [19,20]. This is due to several factors. First, Algiers possesses significantly varied geographic and environmental features, such as elevation and proximity to the sea, where the most populated areas are located. Second, those areas are found within old urban fabrics, characterized by narrow, often covered streets, and colonial-era buildings with arcades providing solar shading. Furthermore, according to a pedestrians' thermal comfort investigation [60], these urban fabrics demonstrate better thermal conditions compared to the other layouts found in the remaining municipalities. This is further supported by [61,62], who indicated that these covered passages and streets consistently offer the best thermal comfort performance across all measurements.

4.2. UTCI Assessment

Algeria, particularly Algiers, is representative of the Mediterranean climate zone, where urban heat dynamics are influenced not only by global climate trends but also by local geographic and environmental factors. Furthermore, it has a very diverse urban layout and morphology along with various land use and building materials all together influencing thermal stress parameters.

The UTCI results from this research showed that during the summer from 2001 to 2023, Algiers was classified in the first period (Figure 8a) as both "no thermal heat stress" and "moderate thermal stress", while in the remaining periods, (Figure 8b–d), it was classified as "moderate thermal stress" and "strong thermal stress", indicating a clear increase in heat stress across Algiers throughout 23 years, which aligns with the global trends due to climate change. Similar findings have been reported in other regions, showing that UTCI values are increasing with time, leading to intense thermal stress experienced by urban populations during extreme heat events [63,64]. However, unlike HHRI, the spatial distribution of UTCI remained stable because the environmental conditions across different districts have not varied significantly over the decades. Moreover, topography has a crucial influence on altering thermal stress levels [65]. The northwestern areas of Algiers, which are situated at higher elevations (Figure 2) had lower UTCI values. This inverse correlation between altitude and thermal stress explains the stability of the UTCI spatial pattern, as the topography of the city has not changed over the study period. The elevated areas have cooler temperatures, which assist in mitigating the impact of heat stress [66], resulting in the observed consistency in the distribution of UTCI within these regions.

4.3. Coupled Index Hotspots

Previous studies [17,19,20,38] have used LST as a proxy for human-perceived thermal conditions. However, the way humans perceive LST is different from their perception of air temperature. In light of this, [19] suggested incorporating air temperatures in heat risk assessment studies. Later, [15] found that it is more appropriate to integrate a combined indicator of air temperature and relative humidity for a better human thermal perception. According to our knowledge, only one study [6] tried to incorporate the UTCI within the HHR assessment by integrating heat stress, social vulnerability, and human exposure, thus neglecting the hazard indicator as a direct measure of the intensity and frequency of extreme heat events. To overcome this limitation, we coupled the HHRI with the UTCI for a more comprehensive identification of high-risk areas, and we then determined hotspots using the Getis-Ord Gi* statistics.

Over the considered period (2001–2023), the coupled index demonstrated greater and different risk areas compared to the HHRI alone. This suggests that the coupling of both indicators enhances the sensitivity of risk assessment, particularly where thermal stress becomes severe in areas affected by heat-related vulnerabilities. Furthermore, synchronization between HHRI and the coupled index hotspots became apparent over time, especially during the last period, indicating that areas with high HHRI levels are also experiencing high levels of thermal stress. The urban structure and population distribution may have reached an amount of balance, where external climate factors are now the main driving factors of further rises in risk. The Pearson correlation matrix (Figure 12) supports this observation, showing a significant positive correlation between HHRI and coupled index with time, particularly during the last period.

The persistent hotspots in central and eastern regions throughout all periods (Figure 13) demonstrate the ongoing risk in these areas. The identification of persistent cold spots in the northern regions, especially at higher altitudes, indicates areas that maintain a certain level of resistance. However, their varying intensity demonstrates that even these sites are not completely protected from increasing temperatures and greater thermal stress.

4.4. Implications and Recommendations

As cities expand, achieving sustainable urban development requires integrating health considerations into urban planning, yet these interconnections remain underexplored in global urban science [67]. The insights gained from coupling HHR with thermal stress and the associated cold/hotspots have significant implications for urban planning and public health. According to Wu et al. [8], the complexity of HHR is influenced by both regional and intra-regional factors and requires policy decisions to be made at multiple levels. Our work addresses these requirements by suggesting a multi-scale strategy. At the national level, this strategy aims to (a) create country-wide guidelines for climate-resilient infrastructure that cities and municipalities across Algeria can adopt including heat mitigation strategies; (b) prepare a national heat action plan involving early-warning systems and emergency response strategies [68–70]; (c) develop a national database that combines the real-time monitoring of meteorological data with statistics regarding heat mortality and morbidity during summer and heatwaves in particularly. At the city scale, the strategy aims to (a) encourage the renovation of existing buildings to enhance thermal comfort and energy efficiency [71]; (b) establish an equal distribution of healthcare services across districts, particularly focusing on areas with high HHRI and low care-bed availability.

Furthermore, the identification of persistent hotspots calls for localized, targeted interventions, such as increasing greenspaces and tree cover [72], with more tree-lined streets [73], implementing green roofs [74], and enhancing urban fabrics with their building materials [75]. Moreover, our strategy improves the municipality's infrastructure ability against extreme heat by enhancing water delivery systems and guaranteeing a consistent energy supply for air conditioning [17]. Finally, it raises public awareness of the symptoms of heat-related illnesses and the necessary behavioral adjustments that might minimize the risk of exposure and vulnerability.

By addressing both environmental and health-related urban vulnerabilities, these insights support the goals of Sustainable Development Goal 3 (Good Health and Well-Being), Goal 11 (Sustainable Cities and Communities), and Goal 13 (Climate Action), reinforcing the role of heat-health risk research in global sustainability efforts.

4.5. Limitations and Future Perspectives of the Study

While this study sets an example of how to combine the IPCC's HHR assessment framework with thermal stress, it introduces several novel contributions, including the coupling of HHRI with UTCI, the use of a high-temporal-resolution dataset spanning over two decades, and the application of hotspot-mapping techniques. Together, these provide a more comprehensive understanding of vulnerable areas during extreme heat conditions that could lead to heat-related mortality and morbidity. It is important to acknowledge certain limitations that may affect the interpretation of the results. First, although Algeria is experiencing rising temperatures, there is a considerable lack of public weather stations regarding its large surface, particularly in the capital, Algiers. Therefore, expanding the meteorological spatial resolution in the province would have improved our scientific understanding regarding improvements in thermal, heatwave, and heat risk mitigation. Furthermore, and in agreement with previous research, there is a lack of city-level data on heat-related mortality and morbidity during summer in general and heatwaves in particular [6,9,13,15,17]. If these data can be gathered at a finer scale in the future, studies should prioritize investigating heat-related mortality and morbidity to validate and improve the accuracy of HHR assessment findings. This could provide further insights into the vulnerabilities among different populations. Finally, many variables, such as data on air-conditioning use and the health conditions of the population, are challenging to gather yet might significantly impact the vulnerability assessment [17,20]. Future research should explore various weighting strategies to enhance the precision and relevance of risk estimates in diverse urban contexts.

In addition, the current study was conducted at the municipal level, which limits the ability to capture micro-scale variations in thermal stress. As a result, local-scale variation in UTCI may be underestimated.

Future studies should consider the integration of microclimatic simulation tools such as ENVI-met or SOLWEIG to more accurately assess intra-urban variability and improve our understanding of heat exposure at finer spatial resolutions.

5. Conclusions

This study conducted a long-term assessment (2001–2023) of heat-related risks in Algiers by integrating the Heat Health Risk Index (HHRI) and the Universal Thermal Climate Index (UTCI). Using the IPCC's risk framework, we evaluated hazard, exposure, and vulnerability, and coupled this with thermal stress analysis through UTCI to improve the sensitivity of heat risk identification. This approach offers a more comprehensive understanding of the relationship between environmental heat and human health vulnerability in urban contexts. Key findings from this study include the following:

- HHRI showed a significant increase over time, reflecting the growing vulnerability of Algiers to extreme heat events
- UTCI increased in Algiers between 2001 and 2023, reaching the strong heat stress category.
- Coupling HHRI with UTCI enhanced the sensitivity and accuracy of heat-related risk assessment.
- The identification of persistent hotspots and cold spots offers crucial insights for targeted climate resilience interventions in the most vulnerable areas.

This work addressed a critical research gap, demonstrating the need to include thermal stress into the traditional HHR framework for a better understanding of the vulnerable areas during extreme heat conditions that could cause heat-related mortality and morbidity. It highlights the value of combining HHR indicators with thermal stress data in informing targeted interventions and policy decisions aimed at enhancing climate resilience in rapidly urbanizing regions like Algiers.

Author Contributions: Conceptualization, D.C.Z., D.B., M.E.M. and S.A.; data curation, D.C.Z.; methodology, D.C.Z. and M.A.E.B.R.; software, D.C.Z. and M.A.E.B.R.; supervision, D.B., M.E.M. and S.A.; visualization, D.C.Z. and M.A.E.B.R.; writing—original draft, D.C.Z.; writing—review and editing, D.C.Z., D.B., M.E.M. and S.A. All authors have read and agreed to the published version of the manuscript.

Funding: This research received no external funding.

Institutional Review Board Statement: Not applicable.

Informed Consent Statement: Not applicable.

Data Availability Statement: The data supporting the findings of this study have been deposited in the Harvard Dataverse repository and can be accessed at https://doi.org/10.7910/DVN/D9WGVN.

Acknowledgments: The authors would like to express their sincere gratitude to Claudia Di Napoli for her valuable insights into heat stress assessment and her expertise in the calculation of the Universal Thermal Climate Index (UTCI), which contributed to the methodological framework of this study.

Conflicts of Interest: The authors declare no conflicts of interest.

Abbreviations

The following abbreviations are used in this manuscript:

E	Exposure
GIS	Geographic Information System
H	Hazard
HHRI	Heat Health Risk Index
IPCC	Intergovernmental Panel on Climate Change
LST	Land Surface Temperature
MENA	Middle East and North Africa Region
MNDWI	Modified Normalized Difference Water Index
MODIS	Moderate Resolution Imaging Spectroradiometer
NDBI	Normalized Difference Building Index
NDVI	Normalized Difference Vegetation Index
NIR	Near Infrared
RED	Red Visible Band
SWIR	Shortwave Infrared
UTCI	Universal Thermal Climate Index
V	Vulnerability

References

1. Semahi, S.; Benbouras, M.A.; Mahar, W.A.; Zemmouri, N.; Attia, S. Development of spatial distribution maps for energy demand and thermal comfort estimation in algeria. *Sustainability* **2020**, *12*, 6066. [CrossRef]
2. Di Napoli, C.; McGushin, A.; Romanello, M.; Ayeb-Karlsson, S.; Cai, W.; Chambers, J.; Dasgupta, S.; Escobar, L.E.; Kelman, I.; Kjellstrom, T.; et al. Tracking the impacts of climate change on human health via indicators: Lessons from the Lancet Countdown. *BMC Public Health* **2022**, *22*, 1–8. [CrossRef] [PubMed]
3. Crichton, D. The risk triangle. *Nat. Disaster Manag.* **1999**, *102*, 102–103.
4. IPCC 6th Assessment Report. Available online: https://www.ipcc.ch/assessment-report/ar6/ (accessed on 28 August 2024).
5. Di Napoli, C.; Romanello, M.; Minor, K.; Chambers, J.; Dasgupta, S.; Escobar, L.E.; Hang, Y.; Hänninen, R.; Liu, Y.; Batista, M.L.; et al. The role of global reanalyses in climate services for health: Insights from the Lancet Countdown. *Meteorol. Appl.* **2023**, *30*, e2122. [CrossRef]
6. Dong, J.; Peng, J.; He, X.; Corcoran, J.; Qiu, S.; Wang, X. Heatwave-induced human health risk assessment in megacities based on heat stress-social vulnerability-human exposure framework. *Landsc. Urban. Plan.* **2020**, *203*, 103907. [CrossRef]
7. Sun, H.; Chen, Y.; Li, K.; Gao, S. Spatio-temporal assessment of heat health risk in Chinese metropolitan cities based on the modified multi-indicators coupled risk framework. *Sustain. Cities Soc.* **2024**, *108*, 105451. [CrossRef]
8. Wu, H.; Xu, Y.; Zhang, M.; Su, L.; Wang, Y.; Zhu, S. Spatially explicit assessment of the heat-related health risk in the Yangtze River Delta, China, using multisource remote sensing and socioeconomic data. *Sustain. Cities Soc.* **2024**, *104*, 105300. [CrossRef]
9. Wu, H.; Zhao, C.; Zhu, Y.; Pan, Y. A multiscale examination of heat health risk inequality and its drivers in mega-urban agglomeration: A case study in the Yangtze River Delta, China. *J. Clean. Prod.* **2024**, *458*, 142528. [CrossRef]
10. Ye, J.; Yang, F. Towards multi-scale and context-specific heat health risk assessment—A systematic review. *Sustain. Cities Soc.* **2025**, *119*, 106102. [CrossRef]
11. Baqa, M.F.; Lu, L.; Guo, H.; Song, X.; Alavipanah, S.K.; Nawaz-Ul-Huda, S.; Li, Q.; Chen, F. Investigating heat-related health risks related to local climate zones using SDGSAT-1 high-resolution thermal infrared imagery in an arid megacity. *Int. J. Appl. Earth Obs. Geoinf.* **2025**, *136*, 104334. [CrossRef]
12. Tomlinson, C.J.; Chapman, L.; E Thornes, J.; Baker, C.J. Including the urban heat island in spatial heat health risk assessment strategies: A case study for Birmingham, UK. *Int. J. Health Geogr.* **2011**, *10*, 42. [CrossRef] [PubMed]
13. Hu, K.; Yang, X.; Zhong, J.; Fei, F.; Qi, J. Spatially Explicit Mapping of Heat Health Risk Utilizing Environmental and Socioeconomic Data. *Environ. Sci. Technol.* **2017**, *51*, 1498–1507. [CrossRef] [PubMed]
14. Chen, Q.; Ding, M.; Yang, X.; Hu, K.; Qi, J. Spatially explicit assessment of heat health risk by using multi-sensor remote sensing images and socioeconomic data in Yangtze River Delta, China. *Int. J. Health Geogr.* **2018**, *17*, 1–15. [CrossRef]
15. Zha, F.; Lu, L.; Wang, R.; Zhang, S.; Cao, S.; Baqa, M.F.; Li, Q.; Chen, F. Understanding fine-scale heat health risks and the role of green infrastructure based on remote sensing and socioeconomic data in the megacity of Beijing, China. *Ecol. Indic.* **2024**, *160*, 111847. [CrossRef]
16. Zhang, W.; Zheng, C.; Chen, F. Mapping heat-related health risks of elderly citizens in mountainous area: A case study of Chongqing, China. *Sci. Total. Environ.* **2019**, *663*, 852–866. [CrossRef]
17. Estoque, R.C.; Ooba, M.; Seposo, X.T.; Togawa, T.; Hijioka, Y.; Takahashi, K.; Nakamura, S. Heat health risk assessment in Philippine cities using remotely sensed data and social-ecological indicators. *Nat. Commun.* **2020**, *11*, 1581. [CrossRef] [PubMed]
18. Zhu, W.; Yuan, C. Urban heat health risk assessment in Singapore to support resilient urban design—By integrating urban heat and the distribution of the elderly population. *Cities* **2023**, *132*, 104103. [CrossRef]
19. Wang, S.; Sun, Q.C.; Huang, X.; Tao, Y.; Dong, C.; Das, S.; Liu, Y. Health-integrated heat risk assessment in Australian cities. *Environ. Impact Assess. Rev.* **2023**, *102*, 107176. [CrossRef]
20. Wang, C.; Ren, Z.; Guo, Y.; Zhang, P.; Hong, S.; Ma, Z.; Hong, W.; Wang, X. Assessing urban population exposure risk to extreme heat: Patterns, trends, and implications for climate resilience in China (2000–2020). Sustain. *Cities Soc.* **2024**, *103*, 105260. [CrossRef]
21. Zhang, C.; Yang, Y.; Yu, L. Assessing urban surface thermal environment and heat health risk in Chinese cities: A twenty-year study. *Urban Clim.* **2025**, *59*, 102304. [CrossRef]
22. McGregor, G.R.; Vanos, J.K. Heat: A primer for public health researchers. *Public Health* **2018**, *161*, 138–146. [CrossRef] [PubMed]
23. Crimmins, A.; Balbus, J.; Gamble, J.L.; Beard, C.B.; Bell, J.E.; Dodgen, D.; Eisen, R.J.; Fann, N.; Hawkins, M.D.; Herring, S.C. The Impacts of Climate Change on Human Health in the United States: A Scientific Assessment. 2016. Available online: http://www.preventionweb.net/publication/impacts-climate-change-human-health-united-states-scientific-assessment (accessed on 28 August 2024).
24. Bröde, P.; Błazejczyk, K.; Fiala, D.; Havenith, G.; Holmér, I.; Jendritzky, G.; Kuklane, K.; Kampmann, B. The universal thermal climate index UTCI compared to ergonomics standards for assessing the thermal environment. *Ind. Health* **2013**, *51*, 16–24. [CrossRef] [PubMed]

25. Hu, J.; Zhou, Y.; Yang, Y.; Chen, G.; Chen, W.; Hejazi, M. Multi-city assessments of human exposure to extreme heat during heat waves in the United States. *Remote Sens. Environ.* **2023**, *295*, 113700. [CrossRef]
26. Mahia, L.; Berkouk, D.; Bouzir, T.A.K.; Pigliautile, I.; Pisello, A.L. Investigating the Relationship between Spatial Morphology, Meteorological Factors, and Elderly People Responses in a Traditional Algerian Village, Sustain. *Cities Soc.* **2025**, *121*, 106212. [CrossRef]
27. Bröde, P.; Fiala, D.; Błażejczyk, K.; Holmér, I.; Jendritzky, G.; Kampmann, B.; Tinz, B.; Havenith, G. Deriving the operational procedure for the Universal Thermal Climate Index (UTCI). *Int. J. Biometeorol.* **2012**, *56*, 481–494. [CrossRef]
28. Coccolo, S.; Kämpf, J.; Scartezzini, J.-L.; Pearlmutter, D. Outdoor human comfort and thermal stress: A comprehensive review on models and standards. *Urban Clim.* **2016**, *18*, 33–57. [CrossRef]
29. Lewis, S.C.; King, A.D.; Perkins-Kirkpatrick, S.E.; Mitchell, D.M. Regional hotspots of temperature extremes under 1.5 °C and 2 °C of global mean warming. *Weather. Clim. Extrem.* **2019**, *26*, 100233. [CrossRef]
30. Wedler, M.; Pinto, J.G.; Hochman, A. More frequent, persistent, and deadly heat waves in the 21st century over the Eastern Mediterranean. *Sci. Total Environ.* **2023**, *870*, 161883. [CrossRef]
31. Ali, E.; Cramer, W.; Georgopoulou, E.; Hilmi, N.J.M.; Le Cozannet, G.; Lionello, P. Cross-Chapter Paper 4: Mediterranean Region. In *Climate Change 2022: Impacts, Adaptation and Vulnerability. Contribution of Working Group II to the Sixth Assessment Report of the Intergovernmental Panel on Climate Change*; Cambridge University Press: Cambridge, UK, 2022. [CrossRef]
32. Hajat, S.; Proestos, Y.; Araya-Lopez, J.-L.; Economou, T.; Lelieveld, J. Current and future trends in heat-related mortality in the MENA region: A health impact assessment with bias-adjusted statistically downscaled CMIP6 (SSP-based) data and Bayesian inference. *Lancet Planet. Health* **2023**, *7*, e282–e290. [CrossRef]
33. GFDRR. Global Facility for Disaster Reduction and Recovery (GFDRR). 2024. Available online: https://www.gfdrr.org/en (accessed on 11 September 2024).
34. Philip, S.; Kew, S.; Vautard, R.; Vahlberg, M.; Singh, R.; Driouech, F.; Lguensat, R.; Barnes, C.; Otto, F. Extreme April Heat in Spain, Portugal, Morocco & Algeria Almost Impossible Without Climate Change. 2023 (pp. 1–11). Available online: http://hdl.handle.net/10044/1/103833 (accessed on 28 August 2024).
35. Zitouni, D.C.; Berkouk, D.; Matallah, M.E.; Attia, S. Dataset for Heat Health Risk and Thermal Comfort Assessment in Algiers (2001–2023). *Harv. Dataverse* **2024**. [CrossRef]
36. Esri. ArcGis Pro. 2023. Available online: https://www.esri.com/fr-fr/arcgis/products/arcgis-pro/overview (accessed on 20 December 2024).
37. Ma, L.; Huang, G.; Johnson, B.A.; Chen, Z.; Li, M.; Yan, Z.; Zhan, W.; Lu, H.; He, W.; Lian, D. Investigating urban heat-related health risks based on local climate zones: A case study of Changzhou in China. *Sustain. Cities Soc.* **2023**, *91*, 104402. [CrossRef]
38. Dong, W.; Liu, Z.; Zhang, L.; Tang, Q.; Liao, H.; Li, X. Assessing Heat Health Risk for Sustainability in Beijing's Urban Heat Island. *Sustainability* **2014**, *6*, 7334–7357. [CrossRef]
39. Huang, H.; Ma, J.; Yang, Y. Spatial heterogeneity of driving factors for urban heat health risk in Chongqing, China: A new identification method and proposal of planning response framework. *Ecol. Indic.* **2023**, *153*, 110449. [CrossRef]
40. Pramanik, S.; Punia, M.; Yu, H.; Chakraborty, S. Is dense or sprawl growth more prone to heat-related health risks? Spatial regression-based study in Delhi, India. *Sustain. Cities Soc.* **2022**, *81*, 103808. [CrossRef]
41. Hua, J.; Zhang, X.; Ren, C.; Shi, Y.; Lee, T.-C. Spatiotemporal assessment of extreme heat risk for high-density cities: A case study of Hong Kong from 2006 to 2016. Sustain. *Cities Soc.* **2021**, *64*, 102507. [CrossRef]
42. Mahia, L.; Berkouk, D.; Bouzir, T.A.K.; Pigliautile, I.; Pisello, A.L. Exploring the Relationship between Elderly Women Responses, Multi-domain Factors, and Street Geometry Indicators: A Case Study in a Mediterranean Context. *Build. Environ.* **2025**, *273*, 112647. [CrossRef]
43. USGS. Earth Explorer. 2024. Available online: https://earthexplorer.usgs.gov (accessed on 1 March 2024).
44. Kestens, Y.; Brand, A.; Fournier, M.; Goudreau, S.; Kosatsky, T.; Maloley, M.; Smargiassi, A. Modelling the variation of land surface temperature as determinant of risk of heat-related health events. *Int. J. Health Geogr.* **2011**, *10*, 7. [CrossRef]
45. Huang, H.; Liu, X.; Ren, L. Analysis of the spatiotemporal mechanism of high temperature on residents' irritability in Beijing based on multiscale geographically weighted regression model. *Front. Ecol. Evol.* **2022**, *10*, 973365. [CrossRef]
46. Krüger, E.; Gobo, J.P.A.; Tejas, G.T.; Souza, R.M.d.S.d.; Neto, J.B.F.; Pereira, G.; Mendes, D.; Di Napoli, C. The impact of urbanization on heat stress in Brazil: A multi-city study. *Urban Clim.* **2024**, *53*, 101827. [CrossRef]
47. Matallah, M.E.; Ahriz, A.; Zitouni, D.C.; Arrar, H.F.; Ben Ratmia, M.A.E.; Attia, S. A methodological approach to evaluate the passive cooling effect of Oasis palm groves. *Sustain. Cities Soc.* **2023**, *99*, 104887. [CrossRef]
48. Khan, A.A. Heat related illnesses: Review of an ongoing challenge. *Saudi Med. J.* **2019**, *40*, 1195. [CrossRef] [PubMed]
49. Aboubakri, O.; Khanjani, N.; Jahani, Y.; Bakhtiari, B. Thermal comfort and mortality in a dry region of Iran, Kerman; a 12-year time series analysis. *Theor. Appl. Clim.* **2020**, *139*, 403–413. [CrossRef]

50. Wu, X.; Liu, Q.; Huang, C.; Li, H. Mapping heat-health vulnerability based on remote sensing: A case study in karachi. *Remote Sens.* **2022**, *14*, 1590. [CrossRef]
51. Blazejczyk, K.; Epstein, Y.; Jendritzky, G.; Staiger, H.; Tinz, B. Comparison of UTCI to selected thermal indices. *Int. J. Biometeorol.* **2012**, *56*, 515–535. [CrossRef]
52. Błażejczyk, K.; Jendritzky, G.; Bröde, P.; Fiala, D.; Havenith, G.; Epstein, Y.; Psikuta, A.; Kampmann, B. An introduction to the universal thermal climate index (UTCI). *Geogr. Pol.* **2013**, *86*, 5–10. [CrossRef]
53. Błażejczyk, K.; Błażejczyk, M. BioKlima—Institute of Geography and Spatial Organization PAS. 2010. Available online: https://www.igipz.pan.pl/bioklima-crd.html (accessed on 11 September 2024).
54. Blazejczyk, K. New climatological and physiological model of the Human Heat Balance outdoor (MENEX) and its applications in bioclimatological studies in different scales. *Zeszyty Instytutu Geografii i Przestrzennego Zagospodarowania PAN* **1994**, *28*, 27–58.
55. Wang, C.; Zhan, W.; Liu, Z.; Li, J.; Li, L.; Fu, P.; Huang, F.; Lai, J.; Chen, J.; Hong, F.; et al. Satellite-based mapping of the Universal Thermal Climate Index over the Yangtze River Delta urban agglomeration. *J. Clean. Prod.* **2020**, *277*, 123830. [CrossRef]
56. Manepalli, U.R.; Bham, G.H.; Kandada, S. Evaluation of hotspots identification using kernel density estimation (K) and Getis-Ord (Gi*) on I-630. In Proceedings of the 3rd International Conference on Road Safety and Simulation, National Academy of Sciences, Indianapolis, IN, USA, 14–16 September 2011; pp. 14–16. Available online: https://onlinepubs.trb.org/onlinepubs/conferences/2011/RSS/2/Manepalli,UR.pdf (accessed on 22 August 2024).
57. Wang, Y.; Chan, A.; Lau, G.N.; Li, Q.; Yang, Y.; Yim, S.H.L. Effects of urbanization and global climate change on regional climate in the Pearl River Delta and thermal comfort implications. *Int. J. Clim.* **2019**, *39*, 2984–2997. [CrossRef]
58. Alioua, N.E.H.; Kemmouche, A. Assessing Urban Expansion of Algiers with Random Forest-Based Multi-Index Using Landsat Imagery. In Proceedings of the 2024 IEEE Mediterranean and Middle-East Geoscience and Remote Sensing Symposium (M2GARSS), Oran, Algeria, 15–17 April 2024; pp. 139–143.
59. Heidari, H.; Mohammadbeigi, A.; Khazaei, S.; Soltanzadeh, A.; Asgarian, A.; Saghafipour, A. Assessment of land use–land cover changes using GIS, remote sensing, and CA–Markov model: A case study of Algiers. *Algeria Appl. Geomat* **2020**. [CrossRef]
60. Talhi, A.; Barlet, A.; Bruneau, D.; Aichour, B. Towards a prediction of outdoor human thermal comfort adapted for designers of urban spaces: Examining UTCI and APCI in the context of Algiers (Algeria). *Int. J. Biometeorol.* **2020**, *64*, 651–662. [CrossRef] [PubMed]
61. Arrar, F.H.; Kaoula, D.; Matallah, M.E.; Abdessemed-Foufa, A.; Taleghani, M.; Attia, S. Quantification of Outdoor Thermal Comfort Levels under Sea Breeze in the Historical City Fabric: The Case of Algiers Casbah. *Atmosphere* **2022**, *13*, 575. [CrossRef]
62. Smail, S.A.; Zemmouri, N.; Djenane, M.; Nikolopoulou, M. Investigating the transient conditions of "Sabat" space and its influence on pedestrian sensations during thermal walks. Algiers' Casbah case study. *Build. Environ.* **2024**, *261*, 111760. [CrossRef]
63. Błażejczyk, K.; Twardosz, R. Secular changes (1826–2021) of human thermal stress according to UTCI in Kraków (southern Poland). *Int. J. Clim.* **2023**, *43*, 4220–4230. [CrossRef]
64. Kuchcik, M.; Błażejczyk, K.; Halaś, A. Long-term changes in hazardous heat and cold stress in humans: Multi-city study in Poland. *Int. J. Biometeorol.* **2021**, *65*, 1567–1578. [CrossRef]
65. Zheng, Z.; Lin, X.; Chen, L.; Yan, C.; Sun, T. Effects of urbanization and topography on thermal comfort during a heat wave event: A case study of Fuzhou, China. *Sustain. Cities Soc.* **2024**, *102*, 105233. [CrossRef]
66. Zhou, D.; Zhao, S.; Liu, S.; Zhang, L.; Zhu, C. Surface urban heat island in China's 32 major cities: Spatial patterns and drivers. *Remote Sens. Environ.* **2014**, *152*, 51–61. [CrossRef]
67. Tonne, C.; Adair, L.; Adlakha, D.; Anguelovski, I.; Belesova, K.; Berger, M.; Brelsford, C.; Dadvand, P.; Dimitrova, A.; Giles-Corti, B.; et al. Defining pathways to healthy sustainable urban development. *Environ. Int.* **2021**, *146*, 106236. [CrossRef]
68. Lowe, D.; Ebi, K.L.; Forsberg, B. Heatwave Early Warning Systems and Adaptation Advice to Reduce Human Health Consequences of Heatwaves. *Int. J. Environ. Res. Public Health* **2011**, *8*, 4623–4648. [CrossRef]
69. Kien, N.D.; My, N.H.D.; Thu, D.T.A.; Tri, T.T.C.; Son, N.H.; Phong, T.K.; Tin, H.C.; Lan, N.H.; Thang, T.B.; The, B.D.; et al. Valuation of a Heatwave Early Warning System for Mitigating Risks Associated with Heat-Related Illness in Central Vietnam. *Sustainability* **2023**, *15*, 15342. [CrossRef]
70. Trahan, A.; Walshe, R.; Mehta, V. Extreme heat, gender, and access to preparedness measures: An analysis of the heatwave early warning system in Ahmedabad, India. *Int. J. Disaster Risk Reduct.* **2023**, *99*, 104080. [CrossRef]
71. Duan, Z.; de Wilde, P.; Attia, S.; Zuo, J. Prospect of energy conservation measures (ECMs) in buildings subject to climate change: A systematic review. *Energy Build.* **2024**, *322*, 114739. [CrossRef]
72. Fahmy, M.; Mahdy, M.; Mahmoud, S.; Abdelalim, M.; Ezzeldin, S.; Attia, S. Influence of urban canopy green coverage and future climate change scenarios on energy consumption of new sub-urban residential developments using coupled simulation techniques: A case study in Alexandria, Egypt. *Energy Rep.* **2020**, *6*, 638–645. [CrossRef]
73. Necira, H.; Matallah, M.E.; Bouzaher, S.; Mahar, W.A.; Ahriz, A. Effect of Street Asymmetry, Albedo, and Shading on Pedestrian Outdoor Thermal Comfort in Hot Desert Climates. *Sustainability* **2024**, *16*, 1291. [CrossRef]

74. Arrar, H.F.; Kaoula, D.; Santamouris, M.; Foufa-Abdessemed, A.; Emmanuel, R.; Matallah, M.E.; Ahriz, A.; Attia, S. Coupling of different nature base solutions for pedestrian thermal comfort in a Mediterranean climate. *Build. Environ.* **2024**, *256*, 111480. [CrossRef]
75. Ben Ratmia, F.Z.; Ahriz, A.; Santi, G.; Bouzaher, S.; Mahar, W.A.; Ben Ratmia, M.A.E.; Matallah, M.E. Street Design Strategies Based on Spatial Configurations and Building External Envelopes in Relation to Outdoor Thermal Comfort in Arid Climates. *Sustainability* **2024**, *16*, 221. [CrossRef]